

# Journal of Materials Chemistry A

Accepted Manuscript



This is an *Accepted Manuscript*, which has been through the Royal Society of Chemistry peer review process and has been accepted for publication.

*Accepted Manuscripts* are published online shortly after acceptance, before technical editing, formatting and proof reading. Using this free service, authors can make their results available to the community, in citable form, before we publish the edited article. We will replace this *Accepted Manuscript* with the edited and formatted *Advance Article* as soon as it is available.

You can find more information about *Accepted Manuscripts* in the [Information for Authors](#).

Please note that technical editing may introduce minor changes to the text and/or graphics, which may alter content. The journal's standard [Terms & Conditions](#) and the [Ethical guidelines](#) still apply. In no event shall the Royal Society of Chemistry be held responsible for any errors or omissions in this *Accepted Manuscript* or any consequences arising from the use of any information it contains.

Cite this: DOI: 10.1039/c0xx00000x

ARTICLE TYPE

www.rsc.org/xxxxxx

## Protected lithium anode with porous Al<sub>2</sub>O<sub>3</sub> layer for lithium-sulfur battery

Hang-Kun Jing, Ling-Long Kong, Sheng Liu, Guo-Ran Li and Xue-Ping Gao\*

*Received (in XXX, XXX) Xth XXXXXXXXXX 20XX, Accepted Xth XXXXXXXXXX 20XX*

DOI: 10.1039/b000000x

The performance of the metallic lithium anode is one of the major factors that affect the cycle stability of lithium-sulfur battery. The protection of lithium anode is extremely essential, especially for lithium-sulfur full-cell. Here, a porous Al<sub>2</sub>O<sub>3</sub> layer is fabricated on the surface of metallic lithium anode by using spin-coating method as protective layer for lithium-sulfur battery. The porous Al<sub>2</sub>O<sub>3</sub> protective layer acts as a stable interlayer and suppresses the side reactions between soluble lithium polysulfides and lithium anode by the direct contact during the charge-discharge process. In addition, the inhomogeneous dissolution-deposition reaction, and the formation of serious cracks on the protected lithium anode are suppressed to a certain extent, which is beneficial to insure the good and stable electrochemical activity of lithium anode. Correspondingly, the sulfur cathode with the protected lithium anode exhibits improved electrochemical performance, accompanied simultaneously with the relatively homogeneous lithium deposition on the anode surface due to the even distribution of Li ion flux via Al<sub>2</sub>O<sub>3</sub> protective layer.

### Introduction

Lithium-sulfur battery has been widely considered as one of the most promising candidates for next generation energy storage devices. Sulfur is low cost, natural abundant and environmentally friendly. Moreover, sulfur offers a large theoretical capacity of 1675 mAh g<sup>-1</sup>, which is an order of magnitude higher than any of conventional cathode materials.<sup>1-5</sup> Despite the extensive investigation for decades, there are still many issues that hinder the practical application of lithium-sulfur battery. There is no doubt that the poor cycle stability is the most serious problem. There are a number of reasons leading to the poor cycle performance, including (a) the poor electronic conductivity of sulfur and Li<sub>2</sub>S/Li<sub>2</sub>S<sub>2</sub> leading to the low sulfur utilization, (b) the “shuttle effect” resulted from the dissolution of lithium polysulfide produced during the discharge/charge process, and (c) the fast degradation of metallic lithium anode.<sup>6-8</sup>

To solve the aforementioned problems, many efforts have been made in recent years, and most of them are focused on the fabrication of sulfur cathodes. Sulfur-carbon composite,<sup>9-17</sup> sulfur-polymer composite<sup>18-22</sup> and sulfur-metal oxide<sup>23</sup> are widely prepared and used as cathode materials. In these methods, sulfur is usually trapped inside the nanopores or shells of carbon/polymer/metal oxide. The designed structure provides an efficient host for confining sulfur and lithium polysulfides, suppressing further the “shuttle effect”. Besides, the electronic conductivity of sulfur cathodes can be enhanced by the various conductive substrates, leading to the improvement of the utilization of active materials. Various electrolytes have also been intensively investigated to improve the cycle stability of sulfur

cathodes. LiNO<sub>3</sub> is widely used as a functional additive in electrolyte for lithium-sulfur battery.<sup>24</sup> Other additives,<sup>25-26</sup> new liquid electrolyte,<sup>27-29</sup> and solid-state electrolyte<sup>30-31</sup> have also been explored. Those approaches are effective to suppress the “shuttle effect” by either forming a passivation layer on the surface of lithium anode or reducing the solubility of lithium polysulfides.<sup>30</sup> Here, the stable lithium anode is essential for maintaining the good cycle stability of lithium-sulfur battery,<sup>32-33</sup> especially for full-cell in the practical application.

As for the lithium anode, one of the most serious and old problems is the formation of lithium dendrites across the anode surface in lithium secondary batteries, as a result of the inhomogeneous dissolution-deposition reaction of metallic lithium anode during cycling. The unavoidable formation of lithium dendrites is the intrinsic cause of the short-circuit and safety issue of lithium secondary batteries.<sup>34-35</sup> In addition, the solid electrolyte interface (SEI) on the surface of lithium anode is unstable due to the continual consumption of fresh lithium anode and electrolyte, leading to the poor cycle performance and low coulombic efficiency.<sup>36-38</sup> Particularly, the most severe problem faced by lithium anode in lithium-sulfur battery is the side reaction between lithium anode and soluble lithium polysulfides and the deposition of insoluble sulfides (Li<sub>2</sub>S/Li<sub>2</sub>S<sub>2</sub>) on lithium anode.<sup>32</sup> The insulated sulfides are hard to be utilized in the subsequent cycles, resulting in the loss of active material and very fast capacity fading.<sup>39</sup> To resolve the problems suffered by lithium anode, some efforts have already been made.<sup>32,39,40-45</sup> For instance, polymers are introduced into the surface of lithium anode to enhance the cycle performance of lithium-sulfur

battery.<sup>42-43</sup> Meanwhile, a novel cell configuration using electrically connected graphite and lithium metal as a hybrid anode is also demonstrated to be to improve the cycle performance.<sup>32</sup> It should be noted that the reducibility of metallic lithium anode is much stronger, which could react with any polymers and damage the polymer protective layer on the surface of lithium anode. Therefore, more effective approaches to fabricate a more stable protective layer on the surface of lithium anode should be developed.

$\text{Al}_2\text{O}_3$  is an electrochemically inactive and ceramic material with a low cost and natural abundance.  $\text{Al}_2\text{O}_3$  coating layer has already been applied on both sulfur cathode<sup>46-48</sup> and separators,<sup>49</sup> which is proved to be effective in enhancing the cycle stability. Herein, in this work, homogeneous  $\text{Al}_2\text{O}_3$  layer as a protective layer is successfully coated on the surface of metallic lithium anode by using a spin-coating method. It is expected that the  $\text{Al}_2\text{O}_3$  protective layer can restrict the side reactions between soluble lithium polysulfides and lithium anode through a combination of physical separation and chemical adsorption of  $\text{Al}_2\text{O}_3$  layer, which can alleviate the lithium corrosion due to the polysulfides attack. As a result, the cycle performance of lithium-sulfur battery with protected lithium anode could be improved.

## Experimental section

### Preparation of the S/C composite cathode

To prepare the S/C composite, porous carbon (PBX51, Cabot Corporation), conductive carbon black (Black pearl-2000, Cabot Corporation) and sublimed sulfur were mixed in the weight ratio of 1.5:1.5:7, and ball-milled for 1 h in a planetary type with rotational speed of 250 rpm  $\text{min}^{-1}$ . The pre-treated mixture was heated at 155 °C for 12 h under Ar atmosphere. The slurry was prepared by mixing as-prepared S/C composite, super P and PVP in the weight ratio of 7:2:1 under vigorous stirring for 12 h with ethanol and water in the weight ratio of 1:1 as dispersant. The slurry was cast on carbon coated Al foil and dried at 60 °C for 12 h. The sulfur content in the S/C composite is 70 % (presented in TG curves in Fig.S1) and the typical sulfur mass loading in the cathode is about 1.1-1.6 mg  $\text{cm}^{-2}$ .

### Preparation of protected lithium anode

$\text{Al}_2\text{O}_3$  (average particle size of 100 nm, Beijing Boyugaoke Co., Ltd) nanoparticles were added to polyvinylidene fluoride (PVDF 6020 Solef) solution with N,N-dimethylformamide (DMF) as a solvent. The weight ratio of  $\text{Al}_2\text{O}_3$ : PVDF was 70:30. The above slurry was vigorously stirred for 10 h under the protection of argon gas to form homogeneous slurry. A spin-coating method was employed to coat the as-prepared slurry on one side of metallic lithium foil inside the glove box. The coating amounts were set to be 0.23, 0.58, and 0.73 mg  $\text{cm}^{-2}$ , respectively. Correspondingly, the thickness of each coating layer was 1.7, 2.5 and 3.7  $\mu\text{m}$ , respectively, which was measured roughly by SEM and shown in Fig. S2.

### Structural characterization

The sulfur content in the S/C composites was determined by using the thermogravimetric analyzer (METTLER TOLEDO, TGA/DSC1) under Ar atmosphere with a heating rate of 10 °C  $\text{min}^{-1}$  from 50 to 800 °C. The surface morphology of the sulfur

cathode and metallic lithium anode were observed using SEM (Supra 55VP). The metallic lithium anode in the cells after cycling for SEM characterization was further washed with DME thoroughly in the glove box.

### Electrochemical measurement

To evaluate the electrochemical performance of the metallic lithium anode, LIR2032-coin type cells were assembled in a glove box under Ar atmosphere, with Celgard 2400 as separator. Cells with fresh lithium anode were also assembled for comparison. The electrolyte was freshly prepared with  $\text{LiN}(\text{SO}_2\text{CF}_3)_2$  (1 M) and anhydrous  $\text{LiNO}_3$  (1 wt%) in a mixed solvent of 1,3-dioxolane (DOL) and dimethoxyethane (DME) (1:1, by volume). The galvanostatic charge-discharge process was performed from 1.7 V to 2.8 V with the LAND-CT2001A instrument (Wuhan Jinnuo, China) at room temperature. The cyclic voltammetry was conducted with a LK 2005 electrochemical workstation at a scan rate of 0.1 mV  $\text{s}^{-1}$ . Electrochemical impedance spectroscopy (EIS) measurements were performed with a Zahner IM6ex electrochemical workstation in the frequency range of 100 MHz to 0.1 Hz at potentiostatic signal amplitude of 5 mV.

## Results and discussion

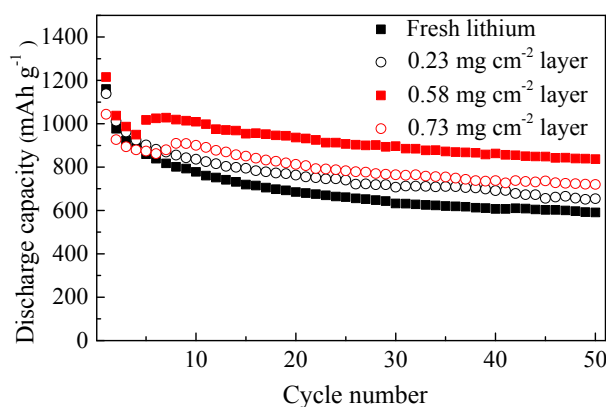


**Fig.1** Cycle performance of lithium-sulfur cells coupled with fresh lithium anode and protected lithium anode at the current density of 160 mA  $\text{g}^{-1}$ .

**Fig.1** shows the cycle performance of lithium-sulfur cells with fresh lithium anode and protected lithium anode with different amounts of  $\text{Al}_2\text{O}_3$  coating layer on lithium anode surface (0.23, 0.58, and 0.73 mg  $\text{cm}^{-2}$ , respectively) at the current density of 160 mA  $\text{g}^{-1}$ . Clearly, the cell coupled with fresh lithium anode shows poor cycle stability. The discharge capacity of sulfur cathode suffers fast decay during the initial 10 cycles, and the capacity retention is about 50 % after 50 cycles. The poor cycle stability is believed to be associated with serious degradation of lithium anode, as proved by the SEM image in following section. When the  $\text{Al}_2\text{O}_3$  layer with different amounts is coated on the surface of lithium anode, the cycle stability and capacity retention of sulfur cathode is significantly improved. In particular, the cell coupled with protected anode with the coating amount of 0.58 mg  $\text{cm}^{-2}$  exhibits the best electrochemical performance. Specifically, the initial capacity of sulfur cathode is 1215 mAh  $\text{g}^{-1}$  and the capacity

retention is about 70 % after 50 cycles. Apparently, the porous  $\text{Al}_2\text{O}_3$  protective layer on the surface of lithium anode is efficient on the improvement of the discharge capacity and cycle stability of sulfur cathode. Usually, the soluble lithium polysulfides in electrolyte would react with lithium anode and result in the loss of active sulfur and the serious degradation of lithium anode, further leading to very fast capacity fading of sulfur cathode. However, the porous  $\text{Al}_2\text{O}_3$  protective layer can restrict the direct contact of soluble lithium polysulfides with lithium anode by both acting as a physical barrier and chemically adsorbing soluble lithium polysulfides, so that the serious degradation of lithium anode is suppressed to certain extent, which is beneficial to the capacity retention of sulfur cathode. It is also noted that the amount of  $\text{Al}_2\text{O}_3$  coating layer on lithium anode is sensitive to the discharge capacity and capacity retention of sulfur cathode. A low amount of  $\text{Al}_2\text{O}_3$  coating layer cannot effectively restrict the direct contact between soluble lithium polysulfides and lithium anode, while a high amount of  $\text{Al}_2\text{O}_3$  coating layer blocks the penetration of electrolyte and the diffusion of lithium ions. Therefore, the optimized amount of  $0.58 \text{ mg cm}^{-2}$  is obtained to achieve the best electrochemical performance. The surface morphology and electrochemical performance of lithium anode with the optimized  $\text{Al}_2\text{O}_3$  protective layer is further investigated in the following sections.

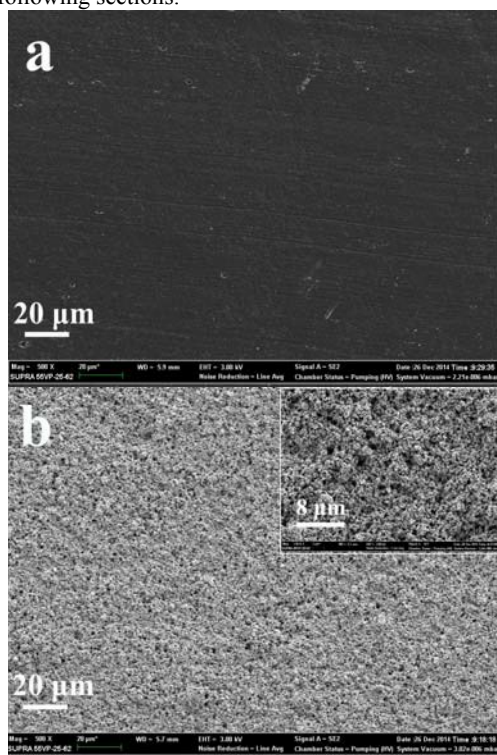


**Fig.2** SEM images of the surface of (a) fresh lithium anode and (b) protected lithium anode with  $\text{Al}_2\text{O}_3$  layer ( $0.58 \text{ mg cm}^{-2}$ ).

The surface morphology of both fresh lithium anode and protected lithium anode before cycling is shown in **Fig. 2**. Here, the surface of metallic lithium foil is pre-treated using a doctor blade to peel off the oxidative layer. It appears that the fresh lithium anode shows the smooth and dense surface morphology (Fig.2a). After coating an  $\text{Al}_2\text{O}_3$  layer with the amount of  $0.58 \text{ mg cm}^{-2}$  by spin-coating method, the surface of lithium anode is completely covered by the homogeneous protective layer (Fig.2b).

Here, the close-packed  $\text{Al}_2\text{O}_3$  nanoparticles are interconnected by the PVDF binder to form the porous structure. The porous structure of  $\text{Al}_2\text{O}_3$  protective layer is considered to be efficient to provide a pathway for the penetration of electrolyte and the diffusion of lithium ions. Meanwhile, the  $\text{Al}_2\text{O}_3$  protective layer can separate the soluble lithium polysulfides and lithium anode from the direct contact.

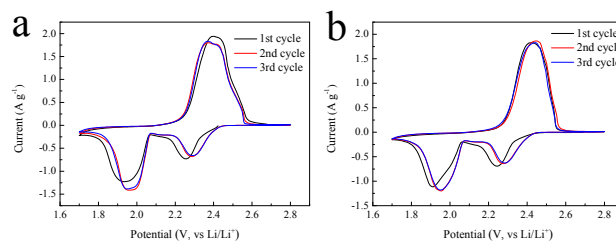


**Fig.3** Cyclic voltammograms of sulfur cathode coupled with (a) fresh lithium anode (b) surface protected lithium anode.

To identify the redox reaction for sulfur cathode coupled with different lithium anodes, cyclic voltammograms (CVs) are presented in **Fig. 3**. For the sulfur cathode coupled with fresh lithium anode and protected lithium anode, there is no obvious difference in the profiles of the redox reaction. During the first cathodic process, two reduction peak potentials appear at around 2.25 V and 1.9 V (vs  $\text{Li/Li}^+$ ), respectively, which could be assigned to the conversion of elemental sulfur to high-order soluble lithium polysulfides and the further reduction of lithium polysulfides to insoluble  $\text{Li}_2\text{S}_2/\text{Li}_2\text{S}$ . In the anodic process, one oxidation peak around 2.4 V (vs  $\text{Li/Li}^+$ ) corresponds to the conversion of  $\text{Li}_2\text{S}_2/\text{Li}_2\text{S}$  to lithium polysulfides, even further to the elemental sulfur. After coating with the protective layer, the initial reduction peaks are slightly shifted to a lower potential, which is ascribed to an increased ohmic resistance, in accordance with the EIS analysis in the following section. In the following cycles, the two reduction peaks and the oxidation peak turn back to normal potentials of sulfur cathode coupled with fresh lithium anode. The potential gap between oxidation and second reduction peaks for sulfur cathode coupled with protected lithium anode is very close to that of sulfur cathode coupled with fresh lithium anode. This is attributed to the decreased potential polarization after activation with the sufficient penetration of electrolyte via the porous  $\text{Al}_2\text{O}_3$  protective layer in the first cycle. It means that the porous  $\text{Al}_2\text{O}_3$  protective layer on the lithium anode does not alter the electrochemical lithium dissolution and deposition reactions.

The charge-discharge profiles of both lithium-sulfur cells at different cycles are presented in **Fig.4**, measured at the current density of  $160 \text{ mA g}^{-1}$ . In the discharge process, two discharge potential plateaus appear around 2.3 V and 2.1 V (vs  $\text{Li/Li}^+$ ), respectively, corresponding to the two step reactions of sulfur with lithium. The similarity of charge-discharge profiles in the first cycle indicates that the protective layer on surface of lithium anode doesn't change the electrochemical reaction process of sulfur cathode, in accordance with CV analysis. For the cell with fresh lithium anode, the potential polarization between the charge potential plateau and the second discharge potential plateau becomes larger with further cycling. Correspondingly, for the cell with protected lithium anode, the lower potential polarization is observed during cycling. Moreover, the discharge capacity

retention is improved for sulfur cathode coupled with protected lithium anode. It is probably due to the protective layer could act as a more stable interlayer and prevent side reactions between soluble lithium polysulfides and lithium anode.

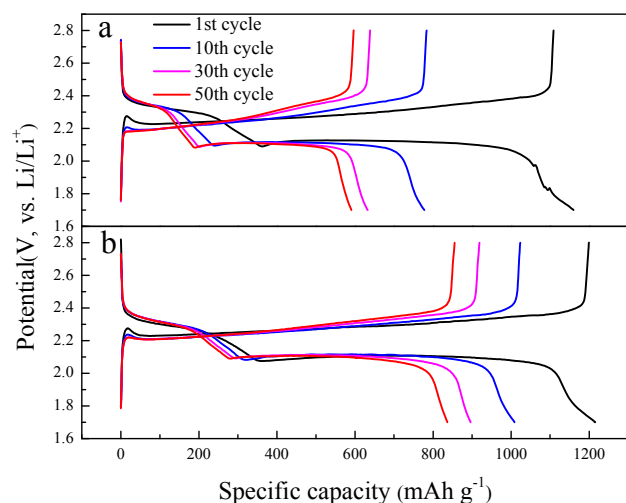


**Fig.4** The potential profiles of lithium-sulfur cells coupled with (a) fresh lithium anode and (b) surface protected lithium anode at the 1st, 10th, 30th, and 50th cycles.

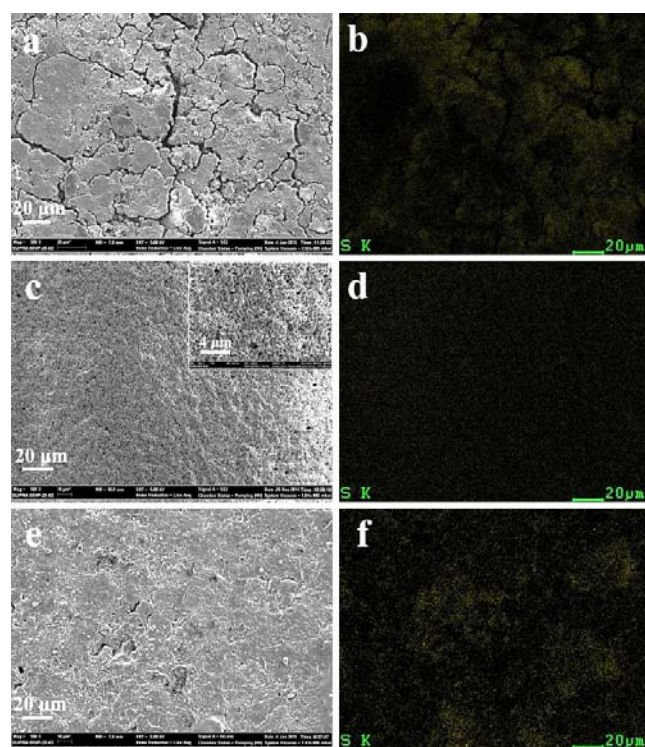


**Fig.5** Surface morphology and elemental mapping of sulfur on lithium anode after 50 cycles: (a, b) fresh lithium anode, (c, d) protected lithium anode with  $\text{Al}_2\text{O}_3$  layer, and (e, f) lithium anode after peeling off the  $\text{Al}_2\text{O}_3$  protective layer.

The surface morphology of the metallic lithium anode with and without the  $\text{Al}_2\text{O}_3$  protective layer in the 50<sup>th</sup> cycle is presented in **Fig.5**. As shown, after 50 cycles, the surface of fresh lithium anode is loose with serious cracks (Fig.5a), coexisting with more sulfur deposition (Fig.5b), which is attributed to the side reactions between lithium anode and soluble lithium polysulfides. In

particular, the serious cracks on lithium surface are more detrimental to the cycle performance of lithium-sulfur battery, especially for full-cells.<sup>27,33,50</sup> The protective layer keeps the almost same morphology before cycling with smooth surface and porous structure (Fig.5c), acting as a stable interlayer during the charge-discharge process. Meanwhile, only a trace of sulfur deposition can be observed on the protective layer (Fig.5d). It means that the protective layer can suppress the side reactions between lithium anode and soluble lithium polysulfides. Moreover, to investigate the surface change of protected lithium anode,  $\text{Al}_2\text{O}_3$  nanoparticles is cautiously removed. It is observed that the surface of lithium anode protected by  $\text{Al}_2\text{O}_3$  layer after 50 cycles is quite smooth with less surface cracks (Fig.5e). It is indicated that the protective layer acts as an interlayer with high uniformity, leading to the even distribution of  $\text{Li}^+$  flux.<sup>51</sup> Therefore, the homogeneous dissolution-deposition process occurs on the lithium anode surface with  $\text{Al}_2\text{O}_3$  protective layer, which is considered to be efficient for the improvement of the cycle performance. Of course, the slight deposition of insulated sulfides is still observed due to the unavoidable diffusion of soluble lithium polysulfides through the porous  $\text{Al}_2\text{O}_3$  layer. Meanwhile, to demonstrate the mechanical stability of the interface, cross-section SEM images of protected lithium anode after initial three cycles at both discharged and charged states are measured and shown in **Fig. S3**. Clearly, the protective layer on lithium anode surface is intact at both discharged and charged states, suggesting that the protective layer is mechanically stable enough to withstand the mechanical strain during the lithium dissolution-deposition process.

The surface morphology of sulfur cathode before and after cycling is provided in **Fig. S4**. The sulfur cathode is consisted of S/C nanoparticles with sizes of 20-40 nm. After 50 cycles, the sulfur cathodes are partially covered with agglomerated  $\text{Li}_2\text{S}_2/\text{Li}_2\text{S}$  discharged products for both cells. In comparison, the sulfur cathode coupled with protected lithium anode shows the relatively good surface integrity after 50 cycles. It indicates that the protection of lithium anode is not only beneficial to the relatively homogeneous lithium deposition on the anode surface, but also to the good surface integrity of sulfur cathode, contributing to the improvement of the cycle stability.

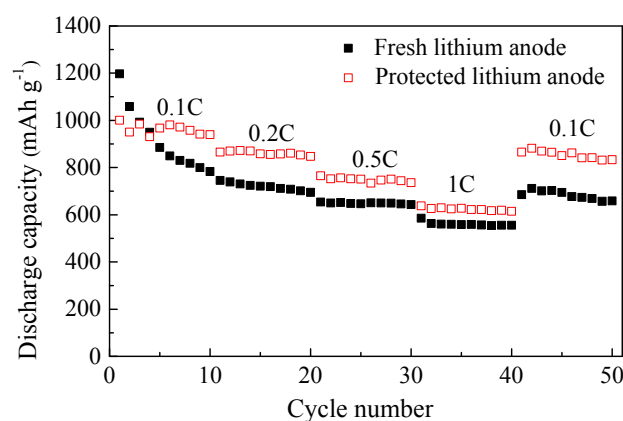


**Fig.6** The rate capability of lithium-sulfur cells with fresh lithium anode and protected lithium anode at different current densities.

To identify the effect of  $\text{Al}_2\text{O}_3$  protective layer on the rate capability of lithium-sulfur cells, the rate discharge capability of

cells with different anodes is investigated at various current densities, as presented in Fig.6. As shown, the discharge capacity of sulfur cathode is gradually decreased with increasing the discharge rates from 0.1C to 1C in both cells. In particular, the discharge rate capability of sulfur cathode coupled with protected lithium anode is still relatively good, even at 1C rate. It means that the porous  $\text{Al}_2\text{O}_3$  protective layer on lithium anode can insure the good rate capability of sulfur cathode.

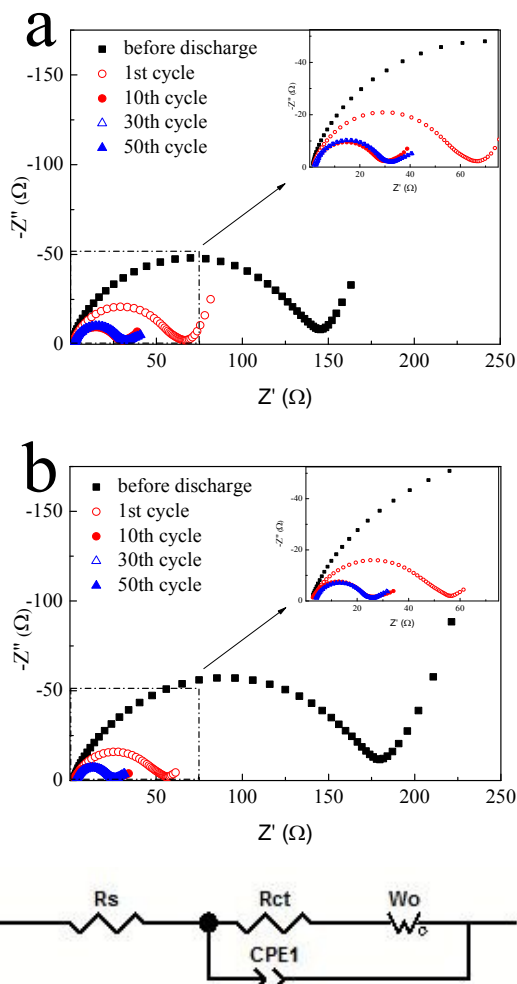


**Fig.7** EIS spectra of the (a) fresh lithium anode (b) protected lithium anode in the cell after charging to 2.8 V at the current density of 160 mA  $\text{g}^{-1}$ . (c) The fitting equivalent circle.

To understand the intrinsic characteristics of the improved electrochemical performance of protected lithium anode, the electrochemical impedance spectra (EIS) of both anodes in different cycles are measured and presented in Fig.7. It is observed that the impedance spectra are composed of a compressed semicircle in the high-frequency region and an inclined line in the low frequency region for both anodes. The compressed semicircle corresponds to the interfacial charge-transfer process, and the inclined line corresponds to a semi-infinite Warburg diffusion process. It means that the electrochemical reaction processes (interfacial charge-transfer and ion diffusion) are almost identical despite of the existence of the porous  $\text{Al}_2\text{O}_3$  protective layer on lithium anode. Before discharging, the ohmic resistance ( $R_s$ ) of solution and interfacial

charge-transfer resistance ( $R_{ct}$ ) of lithium anode are larger for protected lithium anode (Table 1), due to the existence of the inactive  $\text{Al}_2\text{O}_3$  protective layer on lithium anode. With increasing the cycle number, the ohmic resistance of solution is gradually increased for both anodes. In comparison to the low ohmic resistance, the interfacial charge-transfer resistance and Warburg diffusion impedance are large and dominant in EIS. The interfacial charge-transfer resistance is decreased quickly before 10 cycles and then increased slightly after 10 cycles for both anodes. Notably, the interfacial charge-transfer resistance is lower for protected lithium anode after initial activation, showing the better electrochemical activity of lithium anode with slight deposition of insulated sulfides. After 10 cycles, the Warburg diffusion impedance is also lower for protected lithium anode, indicating that Li ions can readily go through the porous  $\text{Al}_2\text{O}_3$  protective layer. Therefore, the porous  $\text{Al}_2\text{O}_3$  protective layer can act as a stable interlayer, and make a contribution to the stable electrochemical activity of lithium anode, in concert with the simultaneous high-performance of sulfur cathode.

**Table 1** The electrochemical parameters simulated from EIS spectra in Fig.7.

Sample	Cycle	$R_s(\Omega)$	$R_{ct}(\Omega)$	$W_o(\Omega)$
Fresh Li anode	0	0.830	134.5	48.44
	1st	1.029	63.93	25.55
	10th	1.877	23.16	26.04
	30th	1.733	24.27	41.79
	50th	2.359	24.32	24.34
Protected Li anode	0	1.683	166.9	51.50
	1st	2.501	46.00	42.86
	10th	2.364	17.13	58.89
	30th	3.506	17.49	21.70
	50th	3.868	19.95	17.89

$R_s$  is the ohmic resistance of solution,  $R_{ct}$  is the interfacial charge-transfer resistance of lithium anode,  $W_o$  is assigned to the semi-infinite Warburg diffusion impedance.

## Conclusion

In summary, uniformly distributed  $\text{Al}_2\text{O}_3$  layer as a protective layer is prepared on the surface of lithium anode by spin-coating method. The effect of the porous  $\text{Al}_2\text{O}_3$  protective layer on the morphology change of lithium anode and electrochemical performance of lithium-sulfur battery is investigated in details. Here, the porous  $\text{Al}_2\text{O}_3$  protective layer can keep the smooth surface morphology of lithium anode with less surface cracks, acting as a stable interlayer during the charge-discharge process. In addition, the surface area exposed on lithium anode is reduced due to the  $\text{Al}_2\text{O}_3$  coating, offering less opportunity for lithium anode to react with the electrolyte and soluble lithium polysulfides. As a result, side reactions between lithium anode and soluble lithium polysulfides are suppressed during cycling, insuring the better electrochemical activity and cycle stability of lithium anode with slight deposition of insulated sulfides.

Correspondingly, the stable electrochemical activity of lithium anode by the porous Al<sub>2</sub>O<sub>3</sub> protective layer is in concert with the simultaneous high-performance of sulfur cathode in lithium-sulfur battery.

## Acknowledgment

Financial Supports from the 973 Program (2015CB251100), NFSC (21421001), and MOE Innovation Team (IRT13022) of China are gratefully acknowledged.

## Notes and references

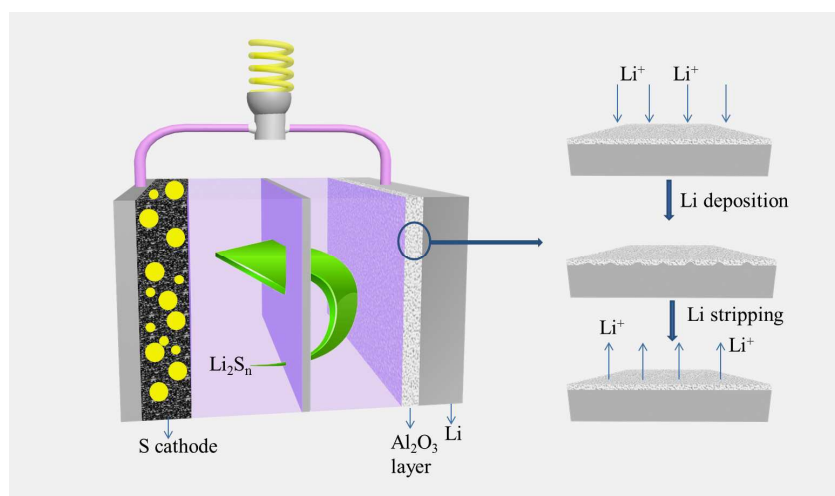
<sup>10</sup> Institute of New Energy Material Chemistry, Collaborative Innovation Center of Chemical Science and Engineering (Tianjin), Tianjin Key Laboratory of Metal and Molecule Based Material Chemistry, Nankai University, Tianjin 300071, China. E-mail: [xpgao@nankai.edu.cn](mailto:xpgao@nankai.edu.cn); Fax: +86-22-2350-0876; Tel: +86-22-23500876

- <sup>1</sup> X. L. Ji and L. F. Nazar, *J. Mater. Chem.*, 2010, **20**, 9821.
- <sup>2</sup> X. P. Gao and H. X. Yang, *Energy Environ. Sci.*, 2010, **3**, 174.
- <sup>3</sup> A. Manthiram, Y. Z. Fu, S. H. Chung, C. X. Zu and Y. S. Su, *Chem. Rev.*, 2014, **114**, 11751.
- <sup>20</sup> <sup>4</sup> P. G. Bruce, S. A. Freunberger, L. J. Hardwick and J. M. Tarascon, *Nat. Mater.*, 2012, **11**, 19.
- <sup>5</sup> G. L. Xu, Q. Wang, J. C. Fang, Y. F. Xu, J. T. Li, L. Huang and S. G. Sun, *J. Mater. Chem. A*, 2014, **2**, 19941
- <sup>6</sup> Y. Yang, G. Zheng and Y. Cui, *Chem. Soc. Rev.*, 2013, **42**, 3018.
- <sup>25</sup> <sup>7</sup> Z. Lin and C. D. Li, *J. Mater. Chem. A*, 2015, **3**, 936.
- <sup>8</sup> G. Y. Xu, B. Ding, J. Pan, P. Nie, L. F. Shen and X. G. Zhang, *J. Mater. Chem. A*, 2014, **2**, 12662.
- <sup>9</sup> B. Zhang, X. Qin, G. R. Li and X. P. Gao, *Energy Environ. Sci.*, 2010, **3**, 1531.
- <sup>30</sup> <sup>10</sup> X. L. Ji, K. T. Lee and L. F. Nazar, *Nat. Mater.*, 2009, **8**, 500.
- <sup>11</sup> X. L. Li, Y. L. Cao, W. Q. L. V. Saraf, J. Xiao, Z. M. Nie, J. Mietek, J. G. Zhang, B. Schwenzer and J. Liu, *J. Mater. Chem.*, 2011, **21**, 16603.
- <sup>12</sup> G. C. Li, G. R. Li, S. H. Ye and X. P. Gao, *Adv. Energy Mater.*, 2012, **2**, 1238.
- <sup>35</sup> <sup>13</sup> W. G. Wang, X. Wang, L. Y. Tian, Y. L. Wang and S. H. Ye, *J. Mater. Chem. A*, 2014, **2**, 4316.
- <sup>14</sup> S. R. Zhao, C. M. Li, W. K. Wang, H. Zhang, M. Y. Gao, X. Xiong, A. B. Wang, K. G. Yuan, Y. Q. Huang and F. Wang, *J. Mater. Chem. A*, 2013, **1**, 3334.
- <sup>40</sup> <sup>15</sup> M. Oschatz, J. T. Lee, H. Kim, W. Nickel, L. Borchardt, W. I. Cho, C. Ziegler, S. Kaskel and G. Yushin, *J. Mater. Chem. A*, 2014, **2**, 17649.
- <sup>16</sup> S. Q. Chen, X. D. Huang, B. Sun, J. Q. Zhang, H. Liu and G. X. Wang, *J. Mater. Chem. A*, 2014, **2**, 16199.
- <sup>45</sup> <sup>17</sup> G. C. Li, J. J. Hu, G. R. Li, S. H. Ye, X. P. Gao, *J. Power Sources*, 2013, **240**, 598.
- <sup>18</sup> W. D. Zhou, Y. C. Yu, H. Chen, F. J. DiSalvo and H. D. Abruna, *J. Am. Chem. Soc.*, 2013, **135**, 16736.
- <sup>19</sup> G. Q. Ma, Z. Y. Wen, J. Jin, Y. Lu, X. W. Wu, C. Liu and C. H. Chen, *RSC Adv.*, 2014, **4**, 21612.
- <sup>50</sup> <sup>20</sup> Y. Yang, G. H. Yu, J. J. Cha, H. Wu, M. Vosgueritchian, Y. Yao, Z. N. Bao and Y. Cui, *ACS Nano*, 2011, **5**, 9187.
- <sup>21</sup> Y. Z. Zhang, S. Liu, G. C. Li, G. R. Li and X. P. Gao, *J. Mater. Chem. A*, 2014, **2**, 4652.
- <sup>55</sup> <sup>22</sup> L. F. Xiao, Y. L. Cao, J. Xiao, B. Schwenzer, M. H. Engelhard, L. V. Saraf, Z. M. Nie, G. J. Exarhos and J. Liu, *J. Mater. Chem. A*, 2013, **1**, 9517.
- <sup>23</sup> Z. W. Seh, W. Y. Li, J. J. Cha, G. Y. Zheng, Y. Yang, M. T. McDowell, P. C. Hsu and Y. Cui, *Nat. Commun.*, 2013, **4**, 1331.
- <sup>60</sup> <sup>24</sup> D. Aurbach, E. Pollak, R. Elazari, G. Salitra, C. S. Kelley and J. Affinito, *J. Electrochem. Soc.*, 2009, **156**, 694.
- <sup>25</sup> F. Wu, J. Qian, R. J. Chen, J. Lu, L. Li, H. M. Wu, J. Z. Chen, T. Zhao, Y. S. Ye and K. Amine, *ACS Appl. Mater. Interfaces*, 2014, **6**, 15542.
- <sup>65</sup> <sup>26</sup> C. X. Zu and A. Manthiram, *J. Phys. Chem. Lett.*, 2014, **5**, 2522.
- <sup>27</sup> J. J. Hu, G. K. Long, S. Liu, G. R. Li and X. P. Gao, *Chem. Commun.*, 2014, **50**, 14647.
- <sup>28</sup> J. W. Park, K. Yamauchi, E. Takashima, N. Tachikawa, K. Ueno, K. Dokko and M. Watanabe, *J. Phys. Chem. C*, 2013, **117**, 4431.
- <sup>70</sup> <sup>29</sup> L. Wang and H. R. Byon, *J. Power Sources*, 2013, **236**, 207.
- <sup>30</sup> Z. Lin, Z. Liu, W. Fu, N. J. Dudney and C. D. Liang, *Angew. Chem. Int. Ed.*, 2013, **52**, 7460.
- <sup>31</sup> S. S. Zhang and D. T. Tran, *J. Mater. Chem. A*, 2014, **2**, 7383.
- <sup>32</sup> C. Huang, J. Xiao, Y. Y. Shao, J. M. Zheng, W. D. Bennett, D. P. Lu, L. V. Saraf, M. Engelhard, L. W. Ji, J. G. Zhang, X. L. Li, G. L. Graff and J. Liu, *Nat. Commun.*, 2014, **5**, 3015.
- <sup>33</sup> J. J. Hu, G. R. Li and X. P. Gao, *J. Inorg. Mater.*, 2013, **28**, 1181.
- <sup>34</sup> D. Aurbach, Y. Cohen, *J. Electrochem. Soc.*, 1996, **143**, 3525.
- <sup>35</sup> F. Ding, W. Xu, G. L. Graff, J. Zhang, M. L. Sushko, X. L. Chen, Y. Y. Shao, M. H. Engelhard, Z. M. Nie, J. Xiao, X. J. Liu, P. V. Sushko, J. Liu and J. G. Zhang, *J. Am. Chem. Soc.*, 2013, **135**, 4450.
- <sup>80</sup> <sup>36</sup> D. Aurbach, *J. Power Sources*, 2000, **89**, 206.
- <sup>37</sup> K. Xu, N. D. Day and C. A. Angell, *J. Electrochem. Soc.*, 1996, **143**, 209.
- <sup>85</sup> <sup>38</sup> W. Xu, J. L. Wang, F. Ding, X. L. Chen, E. Nasybulin, Y. H. Zhang and J. G. Zhang, *Energy Environ. Sci.*, 2014, **7**, 513
- <sup>39</sup> G. Q. Ma, Z. Y. Wen, M. F. Wu, C. Shen, Q. S. Wang, J. Jin and X. W. Wu, *Chem. Commun.*, 2014, **50**, 14209.
- <sup>40</sup> X. L. Zhang, W. K. Wang, A. B. Wang, Y. Q. Huang, K. G. Yuan, Z. B. Yu, J. Y. Qiu and Y. S. Yang, *J. Mater. Chem. A*, 2014, **2**, 11660.
- <sup>90</sup> <sup>41</sup> J. Bruckner, S. Thieme, F. Bottger-Hiller, I. Bauer, H. T. Grossmann, P. Strubel, H. Althues, S. Spange and S. Kaskel, *Adv. Funct. Mater.*, 2014, **24**, 1284.
- <sup>42</sup> Y. M. Lee, N. S. Choi, J. H. Park and J. K. Park, *J. Power Sources*, 2003, **119-121**, 964.
- <sup>95</sup> <sup>43</sup> G. Q. Ma, Z. Y. Wen, Q. S. Wang, C. Shen, J. Jin and X. W. Wu, *J. Mater. Chem. A*, 2014, **2**, 19355.
- <sup>44</sup> M. Hagen, E. Quiroga-Gonzalez, S. Dorfler, G. Fahrner, J. Tubke, M. J. Hoffmann, H. Althues, R. Speck, M. Krampfert, S. Kaskel and H. Foll, *J. Power Sources*, 2014, **248**, 1058.
- <sup>100</sup> <sup>45</sup> Y. Yan, Y. X. Yin, S. Xin, J. Su, Y. G. Guo and L. J. Wan, *Electrochim. Acta*, 2013, **91**, 58.
- <sup>46</sup> X. G. Han, Y. H. Xu, X. Y. Chen, Y. C. Chen, N. Weadock, J. Y. Wan, H. L. Zhu, Y. L. Liu, H. Q. Li, G. Rubloff, C. S. Wang and L. B. Hu, *Nano Energy*, 2013, **2**, 1197.
- <sup>105</sup> <sup>47</sup> M. P. Yu, W. J. Yuan, C. Li, J. D. Hong and G. Q. Shi, *J. Mater. Chem. A*, 2014, **2**, 7360.
- <sup>48</sup> X. Li, A. Lushington, J. Liu, R. Y. Li and X. L. Sun, *Chem. Commun.*, 2014, **50**, 9757.
- <sup>110</sup> <sup>49</sup> Z. Y. Zhang, Y. Q. Lai, Z. A. Zhang, K. Zhang, J. Li, *Electrochim. Acta*, 2014, **129**, 55.
- <sup>50</sup> S. S. Zhang, *J. Power Sources*, 2013, **231**, 153.
- <sup>51</sup> H. K. Lee, D. J. Lee, Y. J. Kim, J. K. Park and H. T. Kim, *J. Power Sources*, 2015, **284**, 103.

# Protected lithium anode with porous $\text{Al}_2\text{O}_3$ layer for lithium-sulfur battery

Hang-Kun Jing, Ling-Long Kong, Sheng Liu, Guo-Ran Li and Xue-Ping Gao\*

TOC



The protected lithium anode with porous  $\text{Al}_2\text{O}_3$  layer is beneficial to improve the cycle stability and capacity retention of lithium-sulfur battery.